Appl. Phys. B 73, 65–70 (2001) / Digital Object Identifier (DOI) 10.1007/s003400100611

Applied Physics B
Lasers
and Optics

Near-infrared cavity enhanced absorption spectroscopy of hot water and OH in an oven and in flames

R. Peeters[1,*], **G. Berden**[1], **G. Meijer**[1,2]

[1] Department of Molecular and Laser Physics, University of Nijmegen, Toernooiveld, 6525 ED Nijmegen, The Netherlands
[2] FOM-Institute for Plasma Physics Rijnhuizen, P.O. Box 1207, 3430 BE Nieuwegein, The Netherlands

Received: 22 February 2001/Revised version: 23 April 2001/Published online: 7 June 2001 –

Abstract. A compact diode laser operating around 1.5 μm was used to measure cavity enhanced absorption spectra of hot water molecules and OH radicals in radiative environments under atmospheric conditions. Spectra of air were measured in an oven at temperatures ranging from 300 K to 1500 K. These spectra contained rovibrational lines from water and OH. The water spectra were compared to simulations from the HITRAN and HITEMP databases. Furthermore, spectra were recorded in the flame of a flat methane/air burner and in an oxyacetylene flame produced by a welding torch. The results show that cavity enhanced absorption spectroscopy provides a sensitive method for rapid monitoring of species in radiative environments.

PACS: 07.57.Ty; 33.20.Ea

In order to have a good understanding of combustion and reaction mechanisms, it is important to know temperature profiles and absolute concentrations of species in flames, ovens, and plasmas. Direct absorption spectroscopy is a non-invasive, line-of-sight technique from which absolute absorption coefficients can be directly obtained. However, a drawback of this method is the lower sensitivity that precludes its use for the measurements of species with low absorption. Higher sensitivities can be obtained by using cavity ring down (CRD) spectroscopy, which nowadays is commonly used in flame and plasma studies [1].

Meijer et al. [2] were the first to use the CRD technique in a flame experiment. They measured the absorption spectrum of OH ($A^2\Sigma^+ \leftarrow X^2\Pi$) in an atmospheric CH_4/air flame using a Bunsen burner. Since then several radicals have been the subject of study in atmospheric flames. The CH radical has been measured in a stabilized flat CH_4/air flame [3], an oxyacetylene flame from a welding torch [4] and a diffusion flame [5]. Furthermore, for OH, predissociation rates [6] and concentration profiles [7] have also been determined in atmospheric flames.

*Corresponding author.
(Fax: +31/243-653-311, E-mail: rudyp@sci.kun.nl)

At atmospheric pressure the flame front is rather thin. As a result, the measurement of concentration profiles of radicals that are only present in this area is complicated. Therefore, most of the CRD flame studies are performed at low background pressures. In different low pressure flames the CH, CH_2, HCO, OH, and NH radicals have been studied extensively [8–15]. A review of the quantitative measurements of absolute concentrations of radicals in flames is given by Cheskis [16].

The above-mentioned experiments were performed in the ultraviolet (UV) and visible (VIS) spectral region, thereby using strong electronic transitions. Although, in general, vibrational transitions are weaker than electronic transitions, there are several attractive features of using transitions in the near-infrared region. In this spectral region many more molecules can be probed; vibrational transitions of various species can be studied in a rather narrow spectral region. Additionally, the Doppler broadening of the spectral lines, which is proportional to the frequency, is 2–10 times smaller in the infrared region than in the UV–VIS region. This demands a linewidth of the laser that is rather narrow, in order to resolve the transitions and in order to circumvent the CRD bandwidth effect, i.e., the effect that the absorption is underestimated, when the laser bandwidth is comparable to, or larger than, the absorption linewidth [1, 17, 18]. Up to now, only a few CRD experiments have been performed in flames in the near-infrared. Overtone transitions of water in atmospheric flames have been measured by Xie et al. [19] around 820 nm. In a low pressure flame, Scherer et al. measured spectra of the OH radical at 1.6 μm [20] and hydrocarbons were studied at 3.3 μm [20, 21].

All the aforementioned CRD experiments were performed with pulsed laser systems. A higher spectral selectivity is obtained with continuous wave (cw) lasers. When switching from a pulsed laser system to a cw laser system, one might think that the low power output of such a laser limits its use in flames due to the strong radiative background. However, the use of an absorption technique such as cw-CRD spectroscopy (see e.g., [22]) or cavity enhanced absorption (CEA) spectroscopy (see e.g., [23]) is perfectly feasible, although only one such experiment has been reported up to

now. With a cw ring dye laser, Campargue et al. have detected SiH_2 at 579 nm in a silane discharge using the cw-CRD scheme [24].

In this paper we report on CEA measurements performed with a cw diode laser at 1.5 μm in radiative environments. The CEA technique, which is related to the CRD technique, is based on the *time-integrated* measurement of the light exiting a high-finesse optical cavity [23]. CEA spectroscopy has been used to measure absorption spectra in the visible and the infrared spectral regions [23, 25–28]. The high-resolution attribute of this technique has been demonstrated by recording absorption spectra of molecules in a molecular beam [23, 29]. The sensitivity under atmospheric conditions ($9 \times 10^{-8}\,\mathrm{cm}^{-1}$) and the linearity of the CEA technique have been studied by Peeters et al. [25].

In the present study, air is heated in an oven, and CEA spectra of water and OH [$X^2\Pi(v' = 2 \leftarrow v'' = 0)$] are measured at different temperatures. The water spectra are compared to simulations, using data from the latest HITRAN and HITEMP databases (HITRAN: high-resolution transmission molecular absorption database; HITEMP is the high temperature analogue) [30]. Furthermore, spectra are recorded in the premixed methane/air flame from a flat-flame burner and in the oxyacetylene flame from a welding torch, both under atmospheric conditions.

1 Experiment

The experimental setup for CEA spectroscopy is depicted in Fig. 1. Light from an external cavity cw diode laser (New Focus 6262; power < 1.5 mW at 1.515 μm, bandwidth < 5 MHz) is coupled into a high-finesse optically stable cavity, while being scanned back and forth mode-hop free over $1\,\mathrm{cm}^{-1}$. Feedback of light into the laser is minimized by a Faraday isolator. The cavity is formed by two highly reflective mirrors separated by a distance d. On the end mirror a piezoelectric transducer is mounted in order to vary the cavity length during the laser scan. The flame or oven is placed inside the cavity. The light exiting the cavity is focused onto a photodiode detector (New Focus Nirvana) by a lens placed directly behind the end mirror. The measured signal is displayed on a 10-bit oscilloscope as a function of the wavelength, providing a "raw" CEA spectrum.

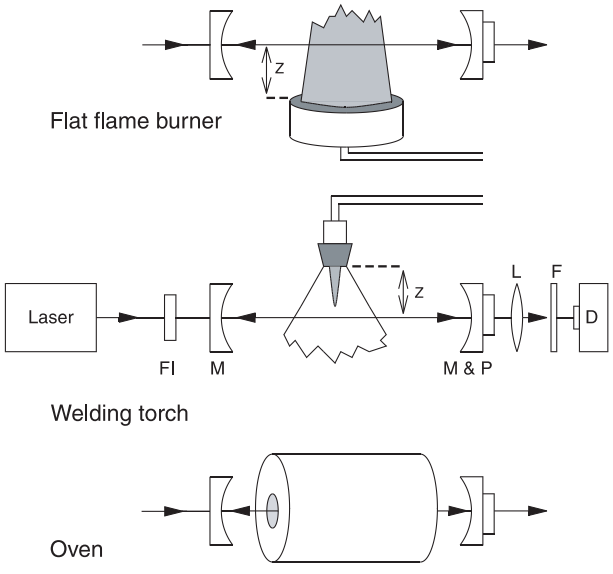

Fig. 1. Schematic of the cavity enhanced absorption experiment. Light from the scanning diode laser is coupled into a high-finesse optical cavity consisting of two highly reflective mirrors (M). A Faraday isolater (FI) prevents feedback into the laser. On the end mirror a piezoelectric transducer (P) is mounted in order to vary the cavity length. A lens (L) focuses the light onto the detector (D). In front of the detector a silicon filter (F) reduces the background radiation. Three different arrangements with the burners and the oven are shown. The distance of the burners relative to the optical axis can be varied

In the following, a short explanation of the CEA technique will be given. A more detailed description has been published elsewhere [23]. If the laser is scanned in frequency (repetition rate of 5 Hz), only those frequencies that are in resonance with the cavity eigenmodes will build up in the optical cavity. The eigenmode structure of the cavity is determined by its geometry (the cavity length d and the radius of curvature r). In CEA the separation between the cavity mirrors is chosen to be $0 < d < r$ or $r < d < 2r$, resulting in a non-confocal cavity having a near-continuum of eigenmodes [2]. Therefore, it is possible to have almost continuous transmission of light through the cavity. However, it is obvious that laser frequencies that are not in resonance with the cavity eigenfrequencies will be blocked. As a consequence, these frequencies will be missing in the final absorption spectrum. In order to couple all frequencies into the cavity, the cavity length is varied (a few micrometers) during the measurement using the piezoelectric transducer (repetition rate 0.5 Hz). Now in each single laser scan the cavity eigenmodes are at different frequencies, allowing other laser frequencies to be transmitted through the cavity. By summing several laser scans on the oscilloscope, laser frequencies are sampled with an equal probability (see also [1]).

In CEA spectroscopy, the total time-integrated signal is proportional to the total cavity losses. The absorption coefficient is given by [1]

$$\kappa(\nu) = \left(\frac{S_0(\nu)}{S(\nu)} - 1\right)\left(\frac{1-R}{l}\right), \tag{1}$$

where $S(\nu)$ is the recorded time-integrated intensity with absorbing species, $S_0(\nu)$ is the CEA signal without absorbing species (i.e., the baseline), R is the reflectivity of the mirrors, and l is the length over which the molecules absorb ($l \leq d$). This equation shows that an absorption spectrum is obtained by dividing the baseline by the CEA signal. Furthermore, this equation shows that the absorption coefficient is expressed in units of $(1 - R)/l$.

One of the most noteworthy advantages of CEA spectroscopy is that a "raw" spectrum appears on the screen of the oscilloscope in a matter of a second. Therefore, it is possible to monitor the species under study "live" with a high sensitivity. As a consequence, changes in absorption due to changes in experimental conditions will become directly visible on the display, which provides great flexibility.

Since the measurements are carried out in radiative environments, the large background radiation intensity has to be suppressed with, for example, filters or a monochromator. The latter approach has been used for measuring hot oxygen in a flame at 628 nm (not shown in this paper). In the present experiments, a silicon high-pass cut-off filter that blocks radi-

ation with wavelengths lower than 1 μm is used. Additionally, the residual background intensity is measured immediately after each single frequency scan in which the "raw" CEA spectrum is recorded. For this an optical shutter, which is closed while the laser is scanned back in frequency, is placed in front of the cavity. The maximum repetition rate of our optical shutter (Melles Griot) is 5 Hz, which limits the data acquisition rate.

In the oven experiment, the optical axis of the cavity is along the center of the bore of the temperature stabilized oven, which can be heated up to 1500 K. The diameter of the bore is 3 cm, and the oven has a length of 25 cm. The oven is open and the measurements are thus performed on laboratory air that is heated inside. Between the cavity mirrors and the oven, diaphragms are placed in order to prevent overheating of the mirrors.

For the flame experiments, the flat burner or welding torch is mounted in such a way that the flame is between the cavity mirrors, while the distance from the burner/torch to the optical axis can be varied. The first flame experiment is performed on a laminar CH_4/air flame of a premixed flat burner [3, 6]. The diameter of the circular burner plate is 3 cm. Mass flow controllers are used to regulate the flow velocity and the gas mixture. A stabilized flame can be obtained by carefully choosing the flame stoichiometry. In this experiment the gas flow velocity is 12 cm/s and the flame has a stoichiometry of $\phi = 1.2$. The second flame experiment is performed in a flame from a commercially available oxy-acetylene welding torch [3, 4], which is normally used for depositing diamond [4]. The torch has an orifice of 1.3 mm and is used to burn oxygen (purity 99.995%) and acetylene (purity 99.6%). The gas flows are regulated with mass flow controllers. In the experiment the flame has a stoichiometry of $\phi = 1.05$ and the oxygen flow is 2.5 L min^{-1}.

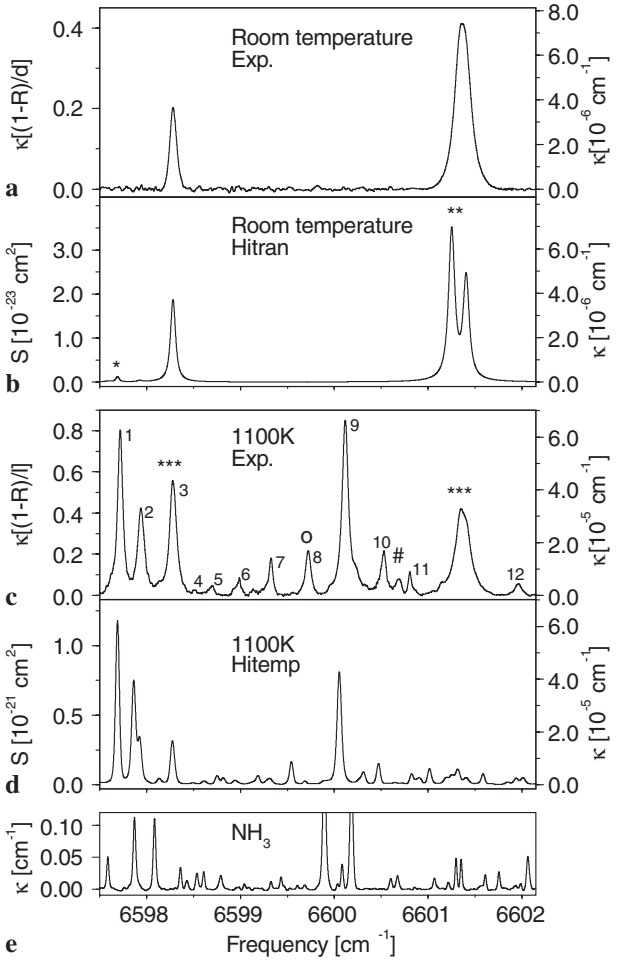

Fig. 2a–e. Spectra of laboratory air around 1.515 μm measured at room temperature and 1100 K and compared with simulations using data from HITRAN or HITEMP. **a** Spectrum at room temperature; both lines originate from water. **b** Simulation of the water spectrum using HITRAN. **c** Spectrum at 1100 K; all water lines except two OH transitions (○, #). The frequencies of the numbered lines are given in Table 1. **d** The corresponding simulation based on HITEMP. **e** Reference spectrum of ammonia used to calibrate the frequency axis of the spectra in **a** and **c**. See text for further details

2 Results and discussion

2.1 Oven

In Fig. 2a the CEA spectrum of water in laboratory air at room temperature, covering $\approx 5\,\mathrm{cm}^{-1}$ around 1.515 μm, is shown. The spectrum consists of 8 overlapping spectra of $1\,\mathrm{cm}^{-1}$, each obtained by summation of 128 laser scans.

The frequency axis is calibrated by simultaneously measuring the direct absorption spectrum of ammonia in a reference cell (Fig. 2e). The spectrum of ammonia is very dense and in each $1\,\mathrm{cm}^{-1}$ scan at least three absorption lines are present. The line positions of the rovibrational ammonia transitions have been measured with a high-resolution Fourier transform infrared absorption spectrometer and have been tabulated by Lundsberg-Nielsen et al. [31]. The absolute frequencies of the ammonia lines are recalibrated using the well-known acetylene absorption lines [32, 33], resulting in a systematic increase in frequency of $0.004(2)\mathrm{cm}^{-1}$ relative to the values tabulated in [31].

On the left vertical axis the absorption coefficient is given in units of $(1 - R)/d$ [23]. Since the length of the cavity is 65 cm, this axis can be put on an absolute scale, provided the reflectivity of the mirrors is known.

In Fig. 2b, the simulation of the water spectrum is shown using data (line position, transition probability and pressure broadening) from the HITRAN database [30]. The contribution of the instrumental broadening of the spectral profile has been determined from low pressure water absorption measurements to be $0.013\,\mathrm{cm}^{-1}$, and it is mainly due to the jittering of the starting position of the laser scans during summation. The right vertical axis, showing the absorption coefficient, κ, is obtained by assuming a relative humidity of 35% (a typical value in our laboratory). From a comparison of the low-frequency water absorption in the measured spectrum to that in the simulated spectrum, an (effective) mirror loss, $1 - R$, of 10^{-3} is determined, which is in good agreement with the loss determined in an independent calibration measurement.

Although at a first glance both spectra seem to be in reasonable agreement, it is evident that there are some discrepancies. The absorption marked with an asterisk in Fig. 2b is not seen in the measured spectrum (not even in a spectrum with a higher signal-to-noise ratio obtained by longer averaging). In the HITRAN database the line position of this absorption is specified to be $6597.690\,\mathrm{cm}^{-1}$, while this

absorption is not tabulated in the paper of Toth [34]. Furthermore, the absorption line marked with two asterisks is not spectrally resolved in the measurement. The position of this line specified in HITRAN is 6601.2510 cm^{-1}, while in the article of Toth [34] the line position is specified to be 6601.3298 cm^{-1}. The latter value clearly is in better agreement with our observations. Additionally, it can be seen that the linewidths of the measured and simulated spectra differ. The linewidths of the simulated spectra can be matched to the measured profiles by assuming a slightly larger air broadening coefficient than specified in HITRAN. The contribution of the self-broadening of water to the spectral linewidth is negligible (for the 6588.281 cm^{-1} absorption this is 0.003 cm^{-1} (HITRAN), whereas the Doppler broadening is 0.020 cm^{-1}).

In Fig. 2c the CEA spectrum measured at 1100 K is shown. The frequencies of the numbered lines in the 1100 K spectrum are given in Table 1. Since the length of the oven (25 cm) is smaller than the length of the cavity (65 cm), the spectrum contains a large contribution from the room-temperature water absorption. Fortunately, this affects only the two spectral features in the 1100 K spectrum marked with three asterisks. Care should be taken to interpret the left vertical scale, because the density and the temperature of the water molecules varies along the cavity axis. Although the length of the oven is 25 cm, the effective absorption path length, l, in which the temperature is 1100 K, is approximately 15 cm [18]. This provides us a way to determine the absorption coefficient (right axis), since $(1-R)/l = 6.7 \times 10^{-5}\,cm^{-1}$.

In Fig. 2d, a simulation of the water spectrum at 1100 K based on data from HITEMP is shown. The absorption axis on the right is obtained by multiplication with the number density at 1100 K (assuming 35% relative humidity at room temperature). As a result, the experimental and simulated spectra can be directly compared. Once again, it should be stressed that the simulated intensities are for 1100 K only, while experimentally there is a temperature gradient present (i.e., outside the oven it is room temperature, while at the center of the oven there is a region at 1100 K). In both spectral discrepancies between the frequency positions of water absorption are clearly visible.

The measured CEA spectrum at 1100 K also contains two transitions originating from the OH radical which is formed by thermal dissociation of water. The spectral feature marked with a hash can be assigned to one component of the $P_1(8)$ doublet of the $X^2\Pi(v' = 2 \leftarrow v'' = 0)$ transition [30, 35]. The other doublet component is marked with a circle. Since both components should have an almost equal intensity [30], it is evident that the component marked with a circle is obscured by interfering water absorption.

Table 1. Frequencies of the numbered lines in the oven spectrum measured at 1100 K (Fig. 2c). The upper limit for the error in the frequency position is 0.005 cm^{-1}

Line no.	Frequency (cm^{-1})	Line no.	Frequency (cm^{-1})
1	6597.719	7	6599.326
2	6579.939	8	6599.722
3	6598.280	9	6600.117
4	6598.511	10	6600.530
5	6598.699	11	6600.805
6	6598.989	12	6601.962

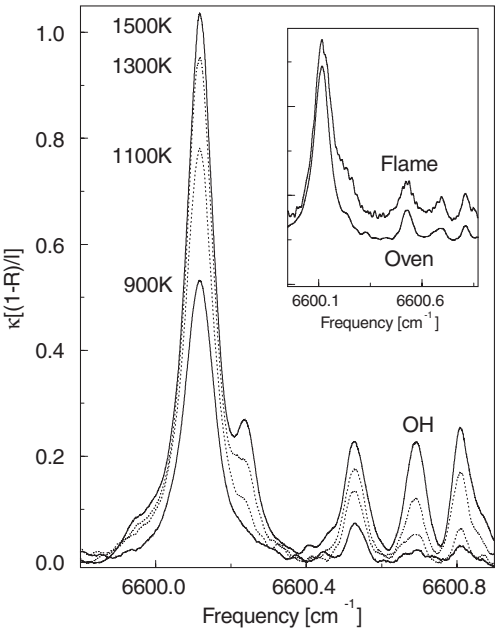

Fig. 3. Part of the hot air spectrum measured at different temperatures. Next to the OH absorption, absorptions from water are present. *Inset*: the 1100 K oven measurement is compared to the scaled spectrum measured in a flame 7.5 cm above the burner surface of the flat burner (see Fig. 4). The spectra are given a vertical offset for clarity

The spectral region including the OH absorption marked with a hash is studied in the oven at different temperatures between 900 and 1500 K. The results are shown in Fig. 3. Although it is not excluded that there are water lines underneath the OH absorption, we can still estimate the OH density. For 1500 K, the integrated absorption is $0.0109 \times (1-R)/l\,cm^{-2}$, with l in cm. The effective path length is smaller than that for water, since the OH number density increases strongly with the temperature. The effective path length l is estimated to be 10 cm [18], giving an integrated absorption of $1.09 \times 10^{-6}\,cm^{-2}$. The line strength at 1500 K is 5.073×10^{-21} cm/molecule [30]. The number density is thus 2.14×10^{14} molecules/cm^3, which corresponds to a concentration of 44 ppm. The temperature dependence of the OH concentration in air has also been studied by Jongma et al. [18]. They used pulsed CRD spectroscopy at 309 nm to probe the OH via the $A^2\Sigma^+(v' = 0) \leftarrow X^2\Pi(v'' = 0)$ transition in the same oven. From their results the concentration of OH at 1500 K is determined to be 34 ppm (at a relative humidity of 35%). The two concentration values compare well, considering that our measurement conditions are not as ideal as those of Jongma et al. [18].

2.2 Flames

The CEA technique is also used to detect OH and water in flames. The CEA spectra in the same spectral region as in Fig. 3 are recorded in the methane/air flame of a flat burner and in the oxyacetylene flame of a welding torch. Measurements are performed at two distances from the burner surface (or orifice) and are shown in Figs. 4 and 5. In a comparison between the oven spectra and the flame spectra, it is evident

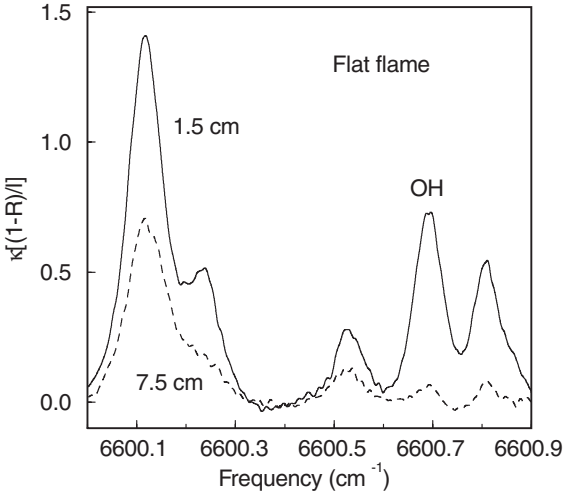

Fig. 4. CEA spectra measured in a methane/air flame at two different heights above the flat burner. The spectral region of these spectra is the same as of those shown in Fig. 3. The spectrum recorded at 7.5 cm above the burner surface compares well to the 1100 K oven spectrum (see inset of Fig. 3)

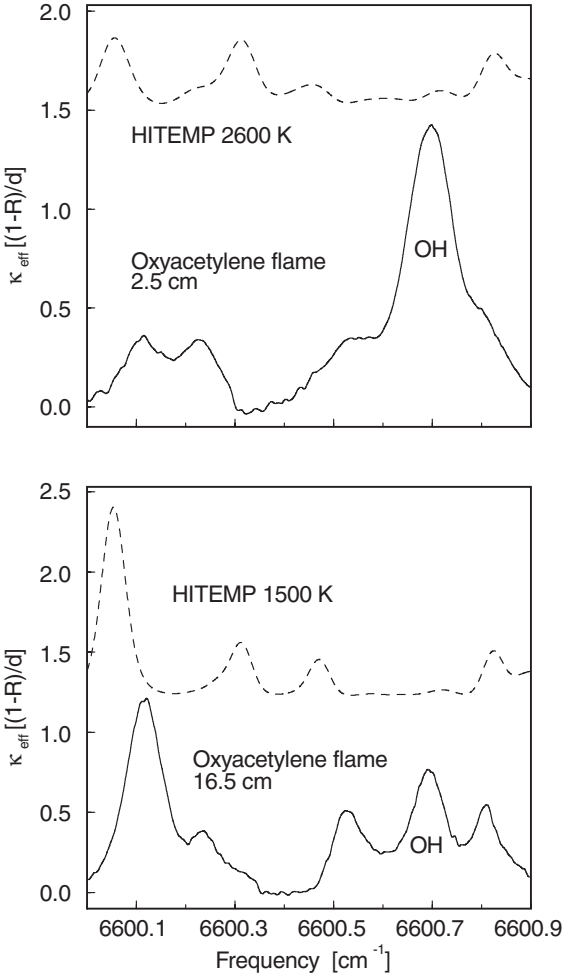

Fig. 5. CEA spectra measured in an oxyacetylene flame from a welding torch for two distances from the burner orifice. The spectral region of these spectra is the same as of those of Figs. 3 and 4. *Dashed lines*: simulated spectra of water based on data from HITEMP. The simulations are scaled to the measured spectra and have been given a vertical offset. Note that the OH absorption is not included in the simulations

that no new (strong) features appear in these flame spectra. Therefore, we assume that all lines in Figs. 4 and 5 solely originate from hot water and OH. The signal-to-noise ratio in the flame measurements is less than that of the oven measurements, due to an increase in the number of fluctuations of the background radiation.

In the experiment with the flat burner, the cavity length, d, is 45 cm, and the length, l, over which the flame extends is 3 cm. The temperature and density distribution can be assumed to be constant over this distance [3]. As a result, a direct comparison can be made between the measurements performed in the flat burner and the aforementioned oven measurements. The inset of Fig. 3 shows the flame spectrum recorded 7.5 cm above the burner plate and the oven spectrum measured at 1100 K. The flame spectrum is scaled to the oven spectrum in order to have the same intensity on the strongest absorption line. Furthermore, the flame spectrum is given a vertical offset for clarity. From the figure it can be seen that both spectra, although measured under different experimental conditions, show a striking resemblance; the relative intensities of the absorption features are the same in both spectra. Therefore, we estimate the temperature in the flat flame to be around 1100 K 7.5 cm above the burner.

It is important to be aware of the fact that the path length, l, is different in both spectra. In the oven measurements, l for water is 15 cm, and for OH it is 10 cm (vide supra), while in the flame measurement it is 3 cm for both molecules. From these measurements a water concentration in the flame (at 7.5 cm) of 2×10^{17} molecules/cm^3 is determined (4.5 times higher than in the 1100 K oven measurement).

In the spectrum obtained 1.5 cm above the burner, both the H_2O and OH absorptions have gained intensity. A comparison of this spectrum to the oven spectra in Fig. 3 shows that the temperature at this point in the flame is higher than 1500 K. Numerical calculations [36] predict a temperature of 1850 K, a water number density of 7.2×10^{17} molecules/cm^3, and an OH number density of about 0.5×10^{15} molecules/cm^3. Assuming this temperature, the OH concentration at 1.5 cm above the burner plate can be calculated from the measurements to be about 3×10^{15} molecules/cm^3. This is about 6 times higher than the value predicted by the numerical calculations [36]. Apart from the fact that there are partially overlapping water lines that slightly complicate the determination of the OH concentration, there is also an uncertainty in the actual settings of the flame parameters (which are inputs for the numerical calculations).

In the oxyacetylene flame experiment the cavity length is 30 cm. Roughly, the flame has a diameter of 0.5 cm just below the orifice of the welding torch, while the diameter rapidly increases to about 10 cm at a distance of 15 cm. The path length, l, is in this case not well defined, since the temperature and density distribution are not constant along the optical axis of the cavity (in contrast to the laminar flame from the flat burner) [3]. Therefore, the vertical axes in Fig. 5 show an effective absorption coefficient of $\kappa_{\mathrm{eff}} = \int_0^{\mathrm{d}} \kappa(x)\,\mathrm{d}x/d$. Note, that this is a normal problem encountered in a line-of-sight measurement.

It is clear, from a comparison of the spectra from the two flames (laminar flame and oxyacetylene flame), that the temperatures in the oxyacetylene flame are much higher than

those in the laminar flame. The data from HITEMP are used to simulate the spectra of hot water in order to give an estimate for the temperature, although we realize that the density of water and the temperature are not constant along the cavity axis. The simulated spectra shown in Fig. 5 are scaled to the measured spectra and are given an offset for clarity. By comparing the frequencies and especially the intensities, the absorption features in the simulations can be correlated to those in the experimental spectra (note that the OH absorption is not included in the simulation). Thus, we estimate the temperature at 16.5 cm to be around 1500 K and at 2.5 cm to be around 2600 K.

3 Summary

In this paper, we have used CEA spectroscopy in the near-infrared to detect water and OH in radiative environments. In a previous study on the detection of ammonia at atmospheric pressures, we have shown a sensitivity of $9 \times 10^{-8}\,\mathrm{cm}^{-1}$ using the same experimental setup, although with mirrors of higher reflectivity $(1 - R) = 3 \times 10^{-4}$ [25]. At this moment our laser has a rather low output power. Therefore, in the present experiment, mirrors with a lower reflectivity are used in order to increase the power transmitted through the cavity. From the oven measurements, we can estimate a sensitivity of $10^{-6}\,\mathrm{cm}^{-1}$. Apart from a decrease due to the lower mirror reflectivity, the lower sensitivity is also caused by turbulent air, scattering losses in flames, and fluctuations in the radiative background (which are not completely eliminated). This decrease in sensitivity is common in experiments performed in flames (see, e.g., [15, 19, 20]).

The spectra of hot water and OH in heated air are measured in an oven as a function of temperature. The water spectra are compared with simulations using the latest data from HITRAN and HITEMP, showing several discrepancies. However, this is not too surprising, since the high-temperature data is primarily based on calculations [30]. Our results show that CEA spectroscopy is a promising technique to obtain experimental data at high temperatures.

The CEA technique is also suited to detect species in flames. We have measured spectra of hot water and OH in two different flames at 1.515 μm. The near-infrared spectral region is attractive since many species have rovibrational transitions here. This offers the possibility of monitoring several species in a limited spectral region. In CEA spectroscopy, a cw laser, having a linewidth of typically a few MHz, is used to excite the molecular transitions. Furthermore, the Doppler broadening is less than in the UV spectral region. Therefore, a high spectral resolution is obtained when detecting molecules with CEA spectroscopy in the near-infrared. In our spectra, for example, OH and water are detected simultaneously in a frequency scan of less than $1\,\mathrm{cm}^{-1}$.

Compared to pulsed CRD or cw-CRD spectroscopy, CEA spectroscopy has the advantage that spectra can be displayed very rapidly without the need for demanding data processing (i.e., for CRD spectroscopy the ring down time must be determined at every frequency). In principle (and as has been demonstrated, for example, by Spence et al. [37]), the sensitivity achievable in cw-CRD spectroscopy is higher than in CEA spectroscopy. Both techniques can be used complimentarily, since all components necessary for performing CEA measurements are also used in cw-CRD spectroscopy. The CEA technique can be used for fast monitoring of species, while the cw-CRD technique can be used whenever the highest sensitivity is required.

Acknowledgements. The authors thank Dr. Nico Dam and Rogier Evertsen for providing the flat flame burner and Ivan Buijnsters for providing the setup for the oxyacetylene flame. Dr. Koen Schreel is acknowledged for providing the results of the numerical calculations.

References

1. G. Berden, R. Peeters, G. Meijer: Int. Rev. Phys. Chem. **19**, 565 (2000)
2. G. Meijer, M.G.H. Boogaarts, R.T. Jongma, A.M. Wodtke, D.H. Parker: Chem. Phys. Lett. **217**, 112 (1994)
3. R. Evertsen, R.L. Stolk, J.J. Ter Meulen: Combust. Sci. Technol. **149**, 19 (1999); ibid. **157**, 341 (2000)
4. R.L. Stolk, J.J. Ter Meulen: Diamond Relat. Mater. **8**, 1251 (1999)
5. X. Mercier, P. Jamette, J.F. Pauwels, P. Desgroux: Chem. Phys. Lett. **305**, 334 (1999)
6. J.J.L. Spaanjaars, J.J. Ter Meulen, G. Meijer: J. Chem. Phys. **107**, 2242 (1997)
7. X. Mercier, E. Therssen, J.F. Pauwels, P. Desgroux: Chem. Phys. Lett. **299**, 75 (1999)
8. I. Derzy, V.A. Lozovsky, S. Cheskis: Chem. Phys. Lett. **306**, 319 (1999)
9. I. Derzy, V.A. Lozovsky, S. Cheskis: Isr. J. Phys. **39**, 49 (1999)
10. A. McIlroy: Chem. Phys. Lett. **296**, 151 (1998)
11. J.W. Thoman, A. McIlroy: J. Phys. Chem. A **104**, 4953 (2000)
12. J.J. Scherer, D.J. Rakestraw: Chem. Phys. Lett. **265**, 169 (1997)
13. A. McIlroy: Isr. J. Phys. **39**, 55 (1999)
14. V.A. Lozovsky, I. Derzy, S. Cheskis: Chem. Phys. Lett. **284**, 407 (1998)
15. S. Cheskis, I. Derzy, A. Kachanov, D. Romanini: Appl. Phys. B **66**, 377 (1998)
16. S. Cheskis: Prog. Energy Comb. Sci. **25**, 233 (1999)
17. P. Zalicki, R.N. Zare: J. Chem. Phys. **102**, 2708 (1995)
18. R.T. Jongma, M.G.H. Boogaarts, I. Holleman, G. Meijer: Rev. Sci. Instrum. **66**, 2821 (1995)
19. J. Xie, B.A. Paldus, E.H. Wahl, J. Martin, T.G. Owano, C.H. Kruger, J.S. Harris, R.N. Zare: Chem. Phys. Lett **284**, 387 (1998)
20. J.J. Scherer, D. Voelkel, D.J. Rakestraw: Appl. Phys. B **64**, 699 (1997)
21. J.J. Scherer, K.W. Aniolek, N.P. Cernanscky, D.J. Rakestraw: J. Chem. Phys. **107**, 6196 (1997)
22. D. Romanini, A.A. Kachanov, N. Sadeghi, F. Stoeckel: Chem. Phys. Lett. **270**, 546 (1997)
23. R. Engeln, G. Berden, R. Peeters, G. Meijer: Rev. Sci. Instrum. **69**, 3763 (1998)
24. A. Campargue, D. Romanini, N. Sadeghi: J. Phys. D **31**, 1168 (1998)
25. R. Peeters, G. Berden, G. Meijer: Appl. Phys. B **71**, 231 (2000)
26. A. O'Keefe, J.J. Scherer, J.B. Paul: Chem. Phys. Lett **307**, 343 (1999)
27. R. Peeters, G. Berden, A. Ólafsson, L.J.J. Laarhoven, G. Meijer: Chem. Phys. Lett. **337**, 231 (2001)
28. H.R. Barry, L. Corner, G. Hancock, R. Peverall, G.A.D. Ritchie: Chem. Phys. Lett. **333**, 285 (2001)
29. G. Berden, R. Peeters, G. Meijer: Chem. Phys. Lett **307**, 131 (1999)
30. http://www.hitran.com
31. L. Lundsberg-Nielsen, F. Hegelund, F.M. Nicolaisen: J. Mol. Spectrosc. **126**, 230 (1993)
32. Q. Kou, G. Guelachvili, M. Abbouti Temsamani, M. Herman: Can. J. Phys. **72**, 1241 (1994)
33. K. Nakagawa, M. de Labachelerie, Y. Awaji, M. Kourogi: J. Opt. Soc. Am. B **13**, 2709 (1996)
34. R.A. Toth: Appl. Opt. **33**, 4851 (1994)
35. W.S. Benedict, E.K. Plyler, C.J. Humphreys: J. Chem. Phys. **21**, 398 (1952)
36. L.M.T. Somers: *The simulation of flat flames with detailed and reduced chemical models*. PhD thesis (Eindhoven University of Technology 1994)
37. T.G. Spence, C.C. Harb, B.A. Paldus, R.N. Zare, B. Willke, R.L. Byer: Rev. Sci. Instrum. **71**, 347 (2000)